

Article

# Novel Quaternary $\text{TlGaSn}_2\text{Se}_6$ Single Crystal as Promising Material for Laser Operated Infrared Nonlinear Optical Modulators

Oleh V. Parasyuk <sup>1</sup>, Volodymyr S. Babizhetskyy <sup>2</sup>, Oleg Y. Khyzhun <sup>3</sup>, Volodymyr O. Levytskyy <sup>2</sup>, Iwan V. Kityk <sup>4,\*</sup> , Galyna L. Myronchuk <sup>5</sup>, Oksana V. Tsisar <sup>1</sup>, Lyudmyla V. Piskach <sup>1</sup>, Jaroslaw Jedryka <sup>4</sup>, Artur Maciag <sup>4</sup> and Michal Piasecki <sup>6,\*</sup> 

<sup>1</sup> Department of Inorganic and Physical Chemistry, Lesya Ukrainka Eastern European National University, Voli Ave. 13, 43025 Lutsk, Ukraine; Parasyuk.Oleg@eenu.edu.ua (O.V.P.); oksana\_tsisar@i.ua (O.V.T.); lyuda0760@ukr.net (L.V.P.)

<sup>2</sup> Department of Inorganic Chemistry, Ivan Franko National University of Lviv, Kyryla and Mefodiya St. 6, 79005 Lviv, Ukraine; fiz\_dekanat@lnu.edu.ua (V.S.B.); v.levytskyy@gmail.com (V.O.L.)

<sup>3</sup> Frantsevych Institute for Problems of Materials Science, National Academy of Sciences of Ukraine, Krzhychanivsky St. 3, 03142 Kyiv, Ukraine; khyzhun@materials.kiev.ua

<sup>4</sup> Institute of Optoelectronics and Measuring Systems, Faculty of Electrical Engineering, Czestochowa University of Technology, Armii Krajowej 17, PL-42-201 Czestochowa, Poland; jaroslaw.jedryka@o2.pl (J.J.); arturmaciag@o2.pl (A.M.)

<sup>5</sup> Physics Department, Lesya Ukrainka Eastern European National University, Voli Ave. 13, 43025 Lutsk, Ukraine; g\_muronchuk@ukr.net

<sup>6</sup> Institute of Physics, J. Dlugosz University, Armii Krajowej 13/15, PL-42201 Czestochowa, Poland

\* Correspondence: iwank74@gmail.com (I.V.K.); m.piasecki@ajd.czyst.pl (M.P.); Tel.: +48-504-274-600 (M.P.)

Academic Editor: Shujun Zhang

Received: 30 September 2017; Accepted: 4 November 2017; Published: 7 November 2017

**Abstract:** The studies of the laser operated third order nonlinear optical features of novel  $\text{TlGaSn}_2\text{Se}_6$  crystal were done. The main efforts were devoted to a search of a possibility to apply these crystals as laser operated optoelectronic material. For this reason, the third harmonic generation of the Nd:YAG pulse laser 1064 nm as the fundamental beam with varied energy density of up to  $200 \text{ J/m}^2$  was studied. As a source of laser operated light, we have used the cw laser (532 nm), exciting the material above the energy gap. Additionally, the influence of middle-energy  $\text{Ar}^+$  ions on the XPS spectra of the  $\text{TlInSn}_2\text{Se}_6$  surface has been explored. We have shown that the main contribution of the  $\text{Se}4p$  states is manifested in the upper part of the valence band of  $\text{TlInSn}_2\text{Se}_6$ . We have established that for the  $\text{TlGaSn}_2\text{Se}_6$  crystal there exists a possibility of variation of the third harmonic generation efficiency using illumination by external continuous wave laser beam. The discovered effect makes it possible to utilize  $\text{TlGaSn}_2\text{Se}_6$  crystal in advanced optoelectronic laser operated devices.

**Keywords:** chalcogenides; crystal structure; electronic structure; XPS; nonlinear optics; photoinduced effects

## 1. Introduction

Before the consideration of the  $\text{TlGaSn}_2\text{Se}_6$  compound, it is necessary to discuss the similar well studied ternary thallium gallium selenide  $\text{TlGaSe}_2$ , which belongs to a known class of  $\text{TlC}^{\text{III}}\text{X}^{\text{VI}}_2$  ferroelectrics semiconductors with layered structure. The later causes strong anisotropy of their parameters [1,2]. The properties of  $\text{TlGaSe}_2$  are currently quite well studied (see, e.g., [3–8]). The material has high photosensitivity, for instance, being used in low-inertia photoresistors as well as in optical analyzers, detectors for visible and IR spectral regions [1,9]. The detector's properties of  $\text{TlGaSe}_2$

were studied in [7,8], and it was shown as a good opportunity to use them for  $\gamma$ - and X-ray radiation (with principal parameters  $\mu\tau_e = 6.0 \times 10^{-5} \text{ cm}^2 \text{ V}^{-1}$ ,  $\mu\tau_h = 9.2 \times 10^{-6} \text{ cm}^2 \text{ V}^{-1}$ ) [8].

It is well known that the improvement of the parameters of such kinds of compounds and consequently their wider application can be attained by the modification with various dopants. This is best achieved by the systematic studies of phase diagrams based on these compounds. When such an approach was applied to the systems  $\text{AgGaS}_2\text{-GeS}_2$  and  $\text{AgGaSe}_2\text{-GeSe}_2$  [10–15] to improve non-linear optical parameters of the ternary compounds  $\text{AgGaS}_2$  and  $\text{AgGaSe}_2$ , it resulted in the synthesis of quaternary chalcogenides  $\text{AgGaGeS}_4$  and  $\text{Ag}_x\text{Ga}_x\text{Ge}_{1-x}\text{Se}_2$ . Like their ternary analog, they also crystallize in the acentric structure, but they have wider transparency windows, higher laser damage threshold (which is particularly important as they are intended for the operating range of the powerful CO- and CO<sub>2</sub>-pulsed lasers), and a simpler crystal growth technique.

As another example, the study of the  $\text{CuInSe}_2\text{-CuGaSe}_2$  system determining the formation of continuous solid solutions series  $\text{CuIn}_{1-x}\text{Ga}_x\text{Se}_2$  (CIGS) is of particular interest. It leads to a significant increase of the photovoltaic parameters of thin film solar cells [16] when compared to those using  $\text{CuInSe}_2$  (CIS). Interesting results were also obtained by us in the study of several  $\text{TlC}^{\text{III}}\text{X}^{\text{VI}}_2$ -based systems. For instance, the  $\text{TlInSe}_2\text{-D}^{\text{IV}}\text{Se}_2$  systems ( $\text{D}^{\text{IV}} = \text{Si, Ge, Sn}$ ) [17,18] exhibit larger solid solution ranges of  $\text{TlInSe}_2$ , the enhanced transport, and better photoelectric and non-linear optical parameters [19–22]. The fundamental difference of the  $\text{TlInSe}_2\text{-D}^{\text{IV}}\text{Se}_2$  systems with respect to many other chalcogenide crystals is the presence of heavy Tl ions which determine the high polarization of the compounds. In addition, chalcogenide complexes provide significant phonon anharmonicities [23] that play an important role in photoinduced IR optical second-order susceptibilities [24]. The particular role for nonlinear optics play is also Li-based ternary/quaternary chalcogenides, which possess high laser damage [25,26].

The chalcogenide crystals studied by us possess a laser damage threshold up to 0.85 GW/cm<sup>2</sup>. At the same time, laser radiation causes irreversible changes that do not exceed 0.3%. Comprehensive studies of photoconductivity, particularly for thallium-bearing compounds, along with calculations of band structure, have shown an essential role of intrinsic cationic defects in the observed effects [19–22] with energy levels within the forbidden energy gap.

In addition to the formation of solid solutions, the  $\text{TlC}^{\text{III}}\text{X}_2^{\text{VI}}\text{-D}^{\text{IV}}\text{X}_2^{\text{VI}}$  systems feature intermediate compounds of several different compositions. The most numerous group are the 1-1-1-4 compounds with the equimolar ratio of the system components. Currently, six such sulphide compounds are known:  $\text{TlInSi}_4$  (SG *Pbmn*) [25],  $\text{TlInGeS}_4$  (dimorphous, SG *Pa3* and *Pnma*) [27],  $\text{TlInSnS}_4$  (SG *P63/mmc*) [28,29],  $\text{TlAlSi}_4$ ,  $\text{TlGaSi}_4$ , and  $\text{TlGaGeS}_4$  (SG *Pbmn*) [30]. The crystal structure is fully determined only for the first three of these compounds. Selenium-containing compounds of equimolar composition exist for all of the  $\text{TlGa(In)Se}_2\text{-D}^{\text{IV}}\text{Se}_2$  cases [17], but for the  $\text{TlInSe}_2\text{-SnSe}_2$  system [18] no intermediate quaternary compounds were found. When testing the formation of the phases of other compositions, a 1-1-2-6 series of compounds was established. The  $\text{TlInSe}_2\text{-GeSe}_2$  system features the  $\text{TlInGe}_2\text{Se}_6$  compound that crystallizes in its own structure type (SG *R3*) [31]. Two other compounds were found in the similar sulfur-containing system,  $\text{TlInGe}_2\text{S}_6$  (SG *R3*) [32] and a 1-1-3-8 composition ( $\text{TlInGe}_3\text{S}_8$  (SG *P21/c*) [33]). The substitution of tin by germanium in the selenide system yielded a new compound,  $\text{TlGaSn}_2\text{Se}_6$ .

In the present work, we present the results of investigations of crystal structure for  $\text{TlGaSn}_2\text{Se}_6$  performed by the X-ray powder method, its electronic structure using X-ray spectroscopy methods, as well as its optical and non-linear optical properties. Studies of the third order nonlinear optical properties of the  $\text{TlGaSn}_2\text{Se}_6$  crystal have shown that the third harmonic generation is sensitive for external photoinducing radiation giving unique material properties, namely an opportunity to manage the third harmonic generation (THG) magnitude by photoinduced radiation.

## 2. Materials and Methods

$\text{TlGaSn}_2\text{Se}_6$  single crystal was grown by melting the batches of high-purity elements (Tl, 99.99 wt. %, Ga, 99.9997 wt. %, Sn, 99.99 wt. %, Se, 99.999 wt. %). The total batch mass was 5 g. The alloy was

synthesized in vacuum evacuated quartz containers (inner diameter 9 mm, length about 100 mm) in a shaft-type furnace by heating to the maximum temperature 1070 K at the rate of 20 K/h, exposure at 1070 K for 6 h, cooling to 670 K at the rate of 10–20 K/h, annealing for 240 h, followed by quenching in air.

A DRON 4-13 diffractometer (Bourestnik, St. Petersburg, Russia) was used for X-ray powder diffraction (PXRD) data collection (45 kV and 30 mA operation conditions, Cu  $K\alpha$ -radiation, Bragg-Brentano geometry). Dark-gray pieces with metallic clusters were ground into fine powder of maroon color using an agate mortar. XRD data were analysed with WinCSD program package [34].

Spectral dependence of the absorption coefficient near the energy gap was measured using non-polarized light of MDR-206 monochromator (LOMO Photonics, St. Petersburg, Russia) in the spectral wavelength range 360–1100 nm. The monochromator resolution was 0.3 nm. The absorption coefficient was calculated similarly to the technique described in [20].

As-grown  $\text{TlInSn}_2\text{Se}_6$  crystal was controlled by the X-ray photoelectron spectroscopy (XPS) technique to clarify the main peculiarities of its electronic structure and chemical bonding. The general features of the present XPS measurements are similar to that employed earlier when studying the related quaternary selenide,  $\text{TlInGe}_2\text{Se}_6$  [29]. Briefly, the present XPS experiments were carried out with UHV-Analysis-System (SPECS Surface Nano Analysis Company, Berlin, Germany). The UHV-Analysis-System is supplied with a hemispherical PHOIBOS 150 analyzer (SPECS Surface Nano Analysis Company, Berlin, Germany). The XPS core-level and valence-band spectra of the  $\text{TlInGe}_2\text{Se}_6$  alloy were excited by a Mg  $K\alpha$  source of X-ray radiation ( $E = 1253.6$  eV) and were registered at fixed pass energy of 30 eV in an ion-pumped chamber having a base pressure of less than  $6 \times 10^{-10}$  mbar. The spectrometer energy scale was calibrated, as described elsewhere [35]. In order to take into account the charging effects, we use the reference C 1s line of adventitious carbon, which the binding energy (BE) was set to be 284.6 eV as it is proposed for respective quaternary Tl-, Ga- and/or Sn-bearing chalcogenides [20,36–38]. We have also measured the X-ray emission (XE) Se  $K\beta_2$  band (transition  $K \rightarrow M_{\text{II,III}}$ ) giving information regarding the energy distribution of the valence Se p states because it is well known that the electronic structure of the quaternary Tl-, Ga-, and/or Sn-bearing selenides is determined substantively by contributions of the Se 4p states forming their valence band region (see, e.g., Refs. [37–39]). The XE Se  $K\beta_2$  band was acquired with an energy resolution of about 0.3 eV using a Johann-type DRS-2M spectrograph, following the technique described in detail in Ref. [40]. In addition, the impact of bombardment with middle-energy  $\text{Ar}^+$  ions on the XPS spectra of the  $\text{TlInGe}_2\text{Se}_6$  alloy surface was also within the scope of the present work, because such treatment is regularly used in epitaxial technologies [31].

### 3. Results and Discussion

#### 3.1. Experimental

##### 3.1.1. Crystal Growth and Structure Determination

Preliminary results on the XRD structure analysis for  $\text{TlGaSn}_2\text{Se}_6$  were presented in the abstract of the presentation at XIII International Conference on Crystal Chemistry of Intermetallic Compounds (Lviv, Ukraine, 2017) [41]. Here, we used more precise equipment with better resolution allowing us to gather statistics for more experimental data. The crystal structure of  $\text{TlGaSn}_2\text{Se}_6$  was refined using initial atomic coordinates of structural type  $\text{TlInGe}_2\text{Se}_6$  (space group  $R3$ ) [42]. Experimental, calculated, and difference powder XRD profiles of the sample with nominal composition corresponding to  $\text{TlGaSn}_2\text{Se}_6$  stoichiometry are shown in Figure 1. Details of the refinement are listed in Table 1. Atomic coordinates and isotropic thermal parameters of the  $\text{TlGaSn}_2\text{Se}_6$  structure are presented in Table 2. Two types of metal atoms arrangement occur in the structure (see Figure 2). The selected inter-atomic distances indicate bonding between the respective atoms and they are shown in Table 3. The charge-balanced electronic formula of  $\text{TlGaSn}_2\text{Se}_6$  reveals the following form:  $\text{Tl}^+\text{Ga}^3+\text{Sn}^{4+}_2\text{Se}^{2-}_6$ . The ionic radii were used when drawing Figure 2 by the DIAMOND program [43].

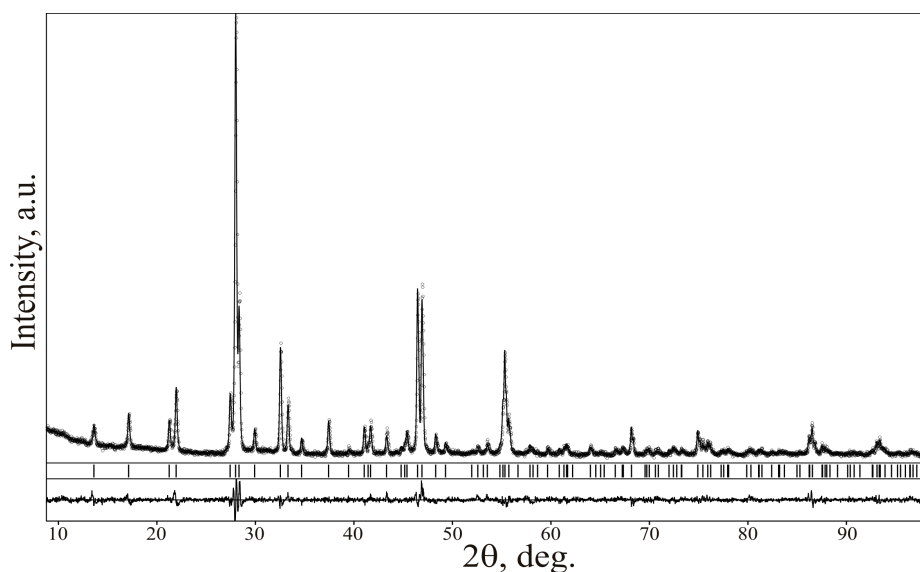


**Figure 1.** Observed (dots) and calculated (solid line) and their difference plot (bottom) of the XRD patterns of TlGaSn<sub>2</sub>Se<sub>6</sub>. Peak positions are marked by short vertical bars.

**Table 1.** Details of the refinement of the crystal structure of TlGaSn<sub>2</sub>Se<sub>6</sub>.

<b>Chemical formula</b>	TlGaSn <sub>2</sub> Se <sub>6</sub>
<b>Space group</b>	R3 (No. 146)
<b>Structure type</b>	TlInGe <sub>2</sub> Se <sub>6</sub>
<b>Pearson symbol and Z</b>	hR30, 3
<b>Unit cell parameters</b>	
<i>a</i> , Å	10.3289(2)
<i>c</i> , Å	9.4340(4)
<i>V</i> , Å <sup>3</sup>	871.64(6)
<b>Calculated density, g cm<sup>-3</sup></b>	5.6301(4)
<b>Diffractometer</b>	DRON 4-13
<b>Radiation, λ</b>	Cu Kα, 1.54185 Å
<b>Mode of refinement</b>	Full with fixed elements per cycle
<b>2θ limits, step; (sinθ/λ)<sub>max</sub></b>	8.80–98.82, 0.02; 0.493
<b>Detector</b>	NaI(Tl) scintillation counter
<b>Scanning time/step, 2θ and sec</b>	0.02, 20
<b>Number of reflections</b>	199
<b>Number of parameters (all/free)</b>	29/5
<b>Scale factor</b>	0.31792(1)
<b>Goodness-of-fit</b>	1.99
<b>R<sub>b(I)</sub>, R<sub>P</sub>, R<sub>Pw</sub></b>	4.8%, 4.1%, 5.4%

**Table 2.** Refined atomic coordinates and isotropic displacement parameters of TlGaSn<sub>2</sub>Se<sub>6</sub> structure.

Atom	Site	<i>X</i>	<i>y</i>	<i>z</i>	<i>B</i> <sub>iso</sub> , Å <sup>2</sup>
Tl	3 <i>a</i>	0	0	0.0000 (5)	1.25 (2)
M	9 <i>b</i>	0.1944 (4)	0.2355 (5)	0.3882 (4)	0.87 (2)
Se1	9 <i>b</i>	−0.0456 (5)	0.2085 (5)	0.2874 (4)	1.11 (2)
Se2	9 <i>b</i>	0.3919 (6)	0.4804 (5)	0.3159 (5)	0.90 (2)

$$M = 1/3\text{Ga} + 2/3\text{Sn}.$$

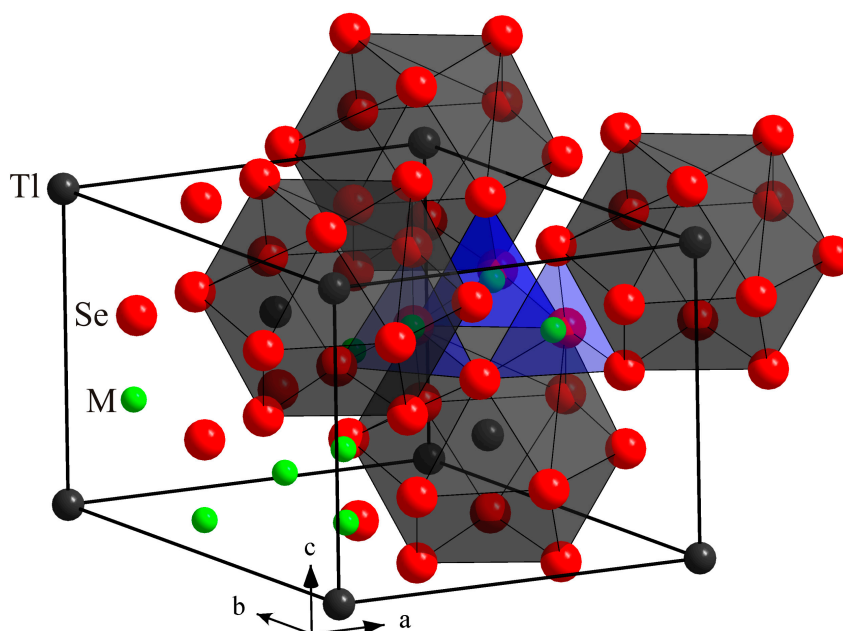


**Figure 2.** General crystallochemistry of  $\text{TlGaSn}_2\text{Se}_6$ . The unit cell and packing of metal atom coordination polyhedra are emphasized.

**Table 3.** Selected inter-atomic distances (in Å) in the  $\text{TlGaSn}_2\text{Se}_6$  structure.

Atoms	Distance	Atoms	Distance
Tl: – 3 Se1	3.636 (5)	M: – Se2	2.422 (7)
3 Se1	3.810 (5)	Se2	2.468 (6)
3 Se2	3.835 (6)	Se1	2.518 (6)
3 Se2	4.022 (6)	Se2	2.537 (6)
Se1: – M	2.518 (6)	Se2: – M	2.422 (7)
M	2.537 (6)	M	2.468 (6)
Tl	3.636 (5)	Tl	3.835 (6)
Tl	3.810 (5)	Tl	4.022 (6)

$$M = 1/3\text{Ga} + 2/3\text{Sn}.$$

### 3.1.2. XPS and XES Data

Survey XPS spectra recorded for as-derived and  $\text{Ar}^+$  ion-irradiated surfaces of the  $\text{TlGaSn}_2\text{Se}_6$  alloy are presented in Figure 3. From this figure, it is evident that all of the spectral peculiarities of the survey XPS data, except for the carbon and oxygen 1s core levels and Auger KLL lines, are well assigned to the core-levels or Auger lines of atoms, which compose the  $\text{TlGaSn}_2\text{Se}_6$  alloy. It is worth mentioning that the relative intensities of the XPS C 1s and O 1s core-level spectra for the pristine surface are relatively small, as Figure 3 depicts. Their origin is a result of adsorption from the air of hydrocarbons and oxygen-containing species because prior to our XPS experiments, the surface of the synthesized  $\text{TlGaSn}_2\text{Se}_6$  alloy was exposed to air over several weeks. It should be mentioned that in the case of the  $\text{TlGaSn}_2\text{Se}_6$  crystal, the Auger Ga  $L_3M_{23}M_{45}$  line is superimposed on the C 1s core-level spectrum, as can be seen from Figure 3. Therefore, in order to overcome the effects of the sample charging during X-ray radiation, we also monitored the binding energy values of measuring core-level spectra employing an electron flood gun, as is recommended in such an occurrence [42–44]. The binding energy of the XPS O 1s core-level spectrum is equal to  $531.9 \pm 0.1$  eV for the as-derived  $\text{TlGaSn}_2\text{Se}_6$  alloy surface, and this binding energy value corresponds to adsorbed oxygen-containing species [43]. However, as can be seen from Figure 3, the  $\text{Ar}^+$  ion-irradiation of the  $\text{TlGaSn}_2\text{Se}_6$  alloy surface causes substantial decreasing of the relative intensities of the XPS C 1s and O 1s core-level spectra.

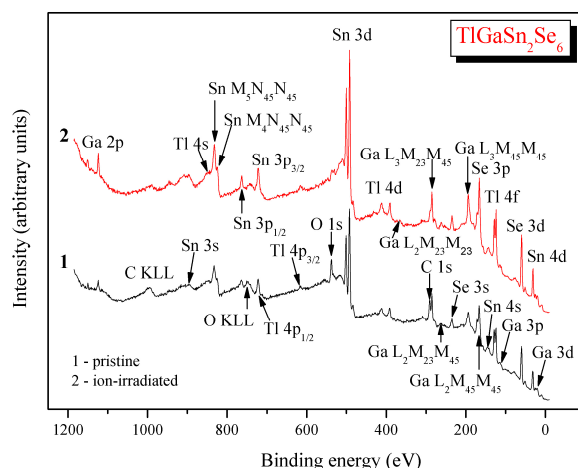


**Figure 3.** Survey X-ray photoelectron spectroscopy (XPS) spectra recorded for (1) pristine and (2)  $\text{Ar}^+$  ion-irradiated surfaces of the  $\text{TlGaSn}_2\text{Se}_6$  alloy.

Figure 4 compiles the most essential XPS core-level spectra related to atoms forming the quaternary selenide under consideration, while binding energy values of the core-level electrons recorded for both surfaces, as-derived and  $\text{Ar}^+$  ion-irradiated, are collected in Table 4. The present XPS results confirm that irradiation of the  $\text{TlGaSn}_2\text{Se}_6$  alloy with 3.0 keV  $\text{Ar}^+$  ions during 5 min (at ion current density installed to be equal to  $14 \mu\text{A}/\text{cm}^2$ ) does not significantly change the values of the binding energies of the core-level electrons related to thallium, gallium and selenium atoms. However, the binding energies of the XPS Sn 3d and Sn 4d core-level electrons decrease by about 0.25 eV in such cases (Table 4). A similar effect was observed previously when studying the influence of the middle-energy  $\text{Ar}^+$  ion-bombardment on other Sn-bearing quaternary selenides.

$\text{Tl}_{1-x}\text{In}_{1-x}\text{Sn}_x\text{Se}_2$  ( $x = 0.1, 0.2, \text{ and } 0.3$ ), namely  $\text{Ag}_2\text{In}_2\text{SiSe}_6$  and  $\text{Ag}_2\text{In}_2\text{GeSe}_6$  [20]. In our opinion, the above-mentioned effect of decreasing the binding energies of the Sn 3d and Sn 4d core-level electrons can be attributed to the removing of a very thin tin oxide species that are formed on the pristine  $\text{TlGaSn}_2\text{Se}_6$  alloy surface due to its exposure to air. Taking into consideration the relative intensities of the XPS Tl  $4f_{7/2}$ , Ga  $3p_{3/2}$ , Sn  $3d_{5/2}$ , and Se 3d core-level lines and the related atomic sensitivity factors (ASF) reported in Ref. [45], we can conclude that in the case of ignoring the presence of carbon and oxygen adsorbed species the  $\text{Ar}^+$  ion-bombardment does not cause visible changes of the stoichiometry of the  $\text{TlGaSn}_2\text{Se}_6$  topmost surface layers. Literature data indicate that the binding energy values for the Sn  $3d_{5/2}$  core-level electrons in highest tin oxide,  $\text{SnO}_2$ , correspond to 286.8–287.0 eV [46,47], which are rather close to those in the  $\text{TlGaSn}_2\text{Se}_6$  alloy under study (see Table 4). As can be seen from the survey spectra presented in Figure 4, the  $\text{Ar}^+$  ion-irradiation induces almost complete elimination of the O 1s core-level line from the  $\text{TlGaSn}_2\text{Se}_6$  alloy surface. The effect of such elimination of a very thin  $\text{SnO}_2$  species is detected in the present XPS experiments, as the above-mentioned decreasing the binding energies of the XPS Sn 3d and Sn 4d core-level electrons in the case of the  $\text{Ar}^+$  ion-bombardment of the  $\text{TlGaSn}_2\text{Se}_6$  alloy surface. Our XPS measurements unambiguously show that the  $\text{Ar}^+$  ion-irradiation does not bring visible changes of the shapes of the XPS core-level spectra (Figure 4), as well as energy distribution of the electronic states within the valence-band region of the  $\text{TlGaSn}_2\text{Se}_6$  alloy (Figure 5). This fact allows us to conclude that the  $\text{TlGaSn}_2\text{Se}_6$  crystalline alloy surface is rather rigid with respect to the influence on it the X-ray irradiation.

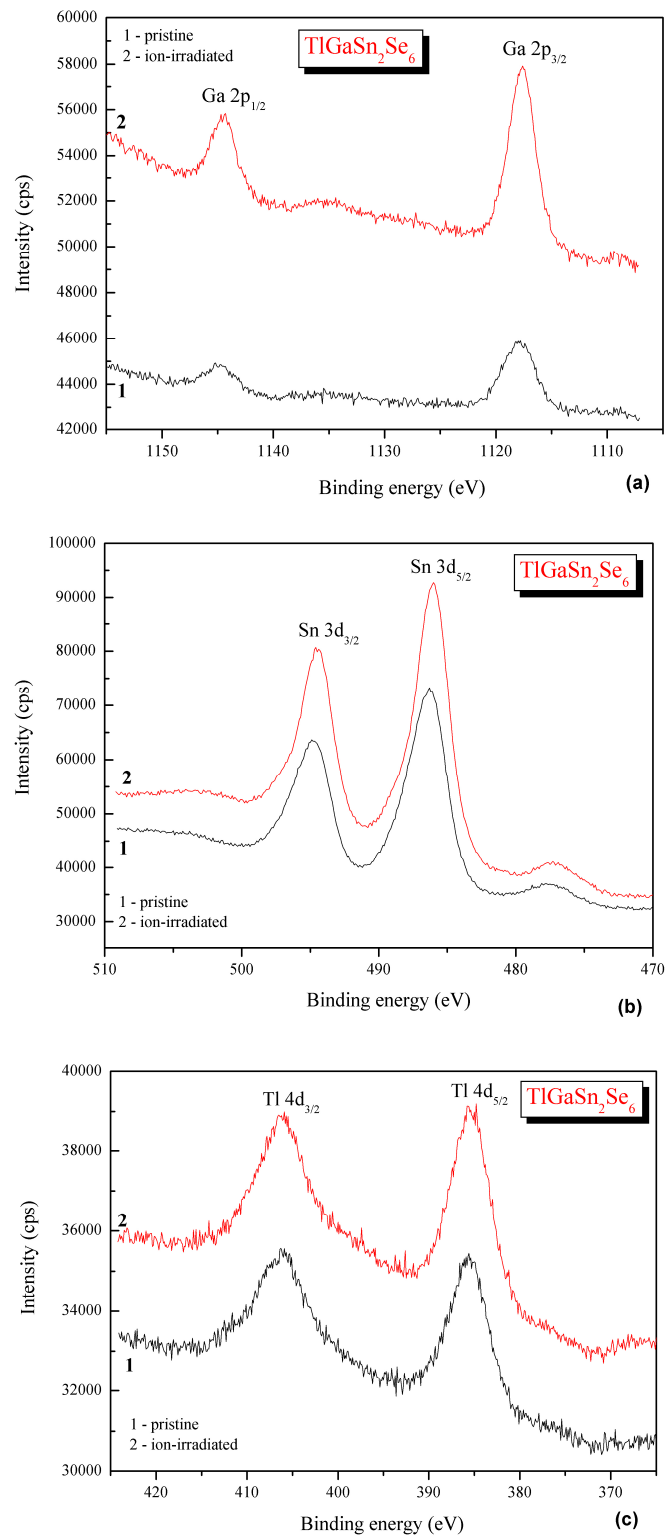
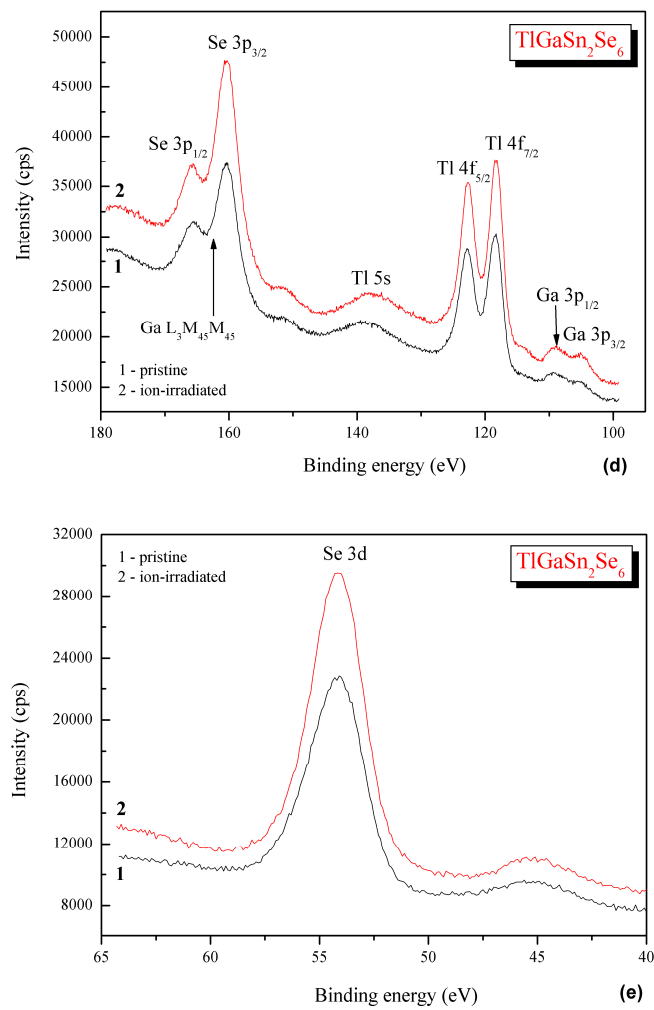


Figure 4. Cont.



**Figure 4.** XPS core-level spectra recorded for: (1) pristine and (2) Ar<sup>+</sup> ion-irradiated surfaces of the TlGaSn<sub>2</sub>Se<sub>6</sub> alloy: (a) Ga 2p; (b) Sn 3d; (c) Tl 4d; (d) Se 3p and Tl 4f (with some nearby core-level spectra and Auger lines); and, (e) Se 3d.

**Table 4.** Binding energies (in eV \*) of constituent element core levels of pristine and bombarded with Ar<sup>+</sup> ions of the TlGaSn<sub>2</sub>Se<sub>6</sub> crystalline surfaces.

Core-Level	TlGaSn <sub>2</sub> Se <sub>6</sub> /Pristine Surface	TlGaSn <sub>2</sub> Se <sub>6</sub> /Ar <sup>+</sup> Ion-Bombarded Surface
Tl 5d <sub>5/2</sub>	113.17	13.26
Ga 3d	19.61	19.66
Sn 4d	25.81	25.57
Se 3d	54.25	54.22
Tl 4f <sub>7/2</sub>	118.44	118.35
Tl 4f <sub>5/2</sub>	122.84	122.77
Se 3p <sub>3/2</sub>	160.47	160.51
Se 3p <sub>1/2</sub>	165.61	165.77
Tl 4d <sub>5/2</sub> **	385.6	385.5
Tl 4d <sub>3/2</sub> **	406.3	406.2
Sn 3d <sub>5/2</sub>	486.35	486.10
Sn 3d <sub>3/2</sub>	494.76	494.52
Ga 2p <sub>3/2</sub> **	1117.8	1117.7
Ga 2p <sub>1/2</sub> **	1144.7	1144.6

\* Uncertainty of the measurements is ±0.05 eV. \*\* Uncertainty of the measurements is ±0.1 eV.

For the  $\text{TlGaSn}_2\text{Se}_6$  alloy, we have also measured the XE Se  $\text{K}\beta_2$  band, bringing information regarding the energy distribution of the Se 4p states and matching it on a common energy scale with the XPS valence band spectrum. The results of such matching the above X-ray photoelectron and emission spectra measured for the  $\text{TlGaSn}_2\text{Se}_6$  alloy following technique [48] are depicted in Figure 6. Following this figure, the spectral maximum of the XES Se  $\text{K}\beta_2$  band is positioned mainly at the upper portion of the XPS valence-band spectrum. Therefore, the principal contributions of the Se 4p states are detected at the upper part of the valence band for the  $\text{TlGaSn}_2\text{Se}_6$  crystal, with the lesser contributions in other parts of the band. Similar peculiarity of the valence band by the Se 4p states is typical for the related quaternary selenide,  $\text{TlInGe}_2\text{Se}_6$ , as it established in Ref. [31]. It is worth mentioning that one can also expect substantial contributions of the Tl s, Sn d, and Ga p electronic states to the valence band of the  $\text{TlGaSn}_2\text{Se}_6$  compound, however, the present available facilities do not allow for recording the energy distribution of these states by our group.

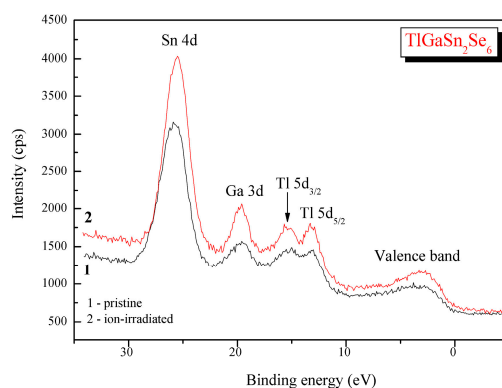


**Figure 5.** XPS valence band spectra recorded for (1) pristine and (2)  $\text{Ar}^+$  ion-irradiated surfaces of the  $\text{TlGaSn}_2\text{Se}_6$  alloy.

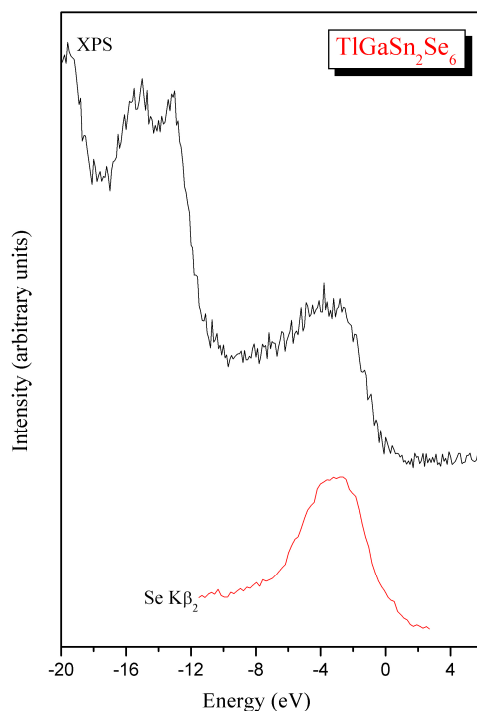


**Figure 6.** Comparison (on a common energy scale) of the XPS valence-band spectrum and the X-ray emission Se  $\text{K}\beta_2$  band of the  $\text{TlGaSn}_2\text{Se}_6$  alloy.

It is well-known that when recording the XPS spectra for chemical elements that constitute semiconductors, they are very sensitive to methods of calibrations of the surface charging effects [45,49]. In such a case, the binding energy difference parameter, e.g.,  $\Delta_{\text{Tl-Se}}$ , which is a difference of the binding energies of the Tl  $4f_{7/2}$  and Se 3d core levels, is not-sensitive to the charging effects [49]. Such a binding energy difference parameter can be effectively used for the determination of ionicity degree of the Tl–Se chemical bonds: a higher value of the  $\Delta$  difference parameter induces an enhanced degree of the ionic component for this chemical bond. From the data listed in Table 4, the difference parameter  $\Delta_{\text{Tl-Se}}$  in the  $\text{TlGaSn}_2\text{Se}_6$  alloy is equal to  $64.19 \pm 0.5$  eV. This value is very close to that of the difference parameter  $\Delta_{\text{Tl-Se}}$  for the related selenide  $\text{TlInGe}_2\text{Se}_6$ , namely 64.1 eV [31]). This means that the ionicity degree of the chemical Tl–Se bonds in the  $\text{TlGaSn}_2\text{Se}_6$  compound corresponds to that in  $\text{TlInGe}_2\text{Se}_6$ .

### 3.1.3. Optical Properties

The spectral distribution of the absorption coefficient is presented in Figure 7a. To obtain the detailed information about the energy band gaps in the crystal, the absorption band edge  $\alpha$  vs. photon energy is analyzed in the high energy absorption regions, where  $E_g$  can be presented by an equation [50]:

$$\alpha h\nu = A(h\nu - E_g)^n \quad (1)$$

where  $A$  is a constant that is determined by the inter-band transition probabilities,  $n$  is a power index characterizing the optical absorption process that (for perfect crystals) is equal to 2 and 1/2 for indirect and direct allowed transitions, respectively. However, this rule is substantially disturbed for the chalcogenide crystals due to presence of a large number of intrinsic cationic defects and exact application of this equation is limited. However, following the presented in Figure 7 dependence, one can see that it is closer to the direct transition [51] (see Figure 7b) with  $E_g^d = 1.86$  eV.

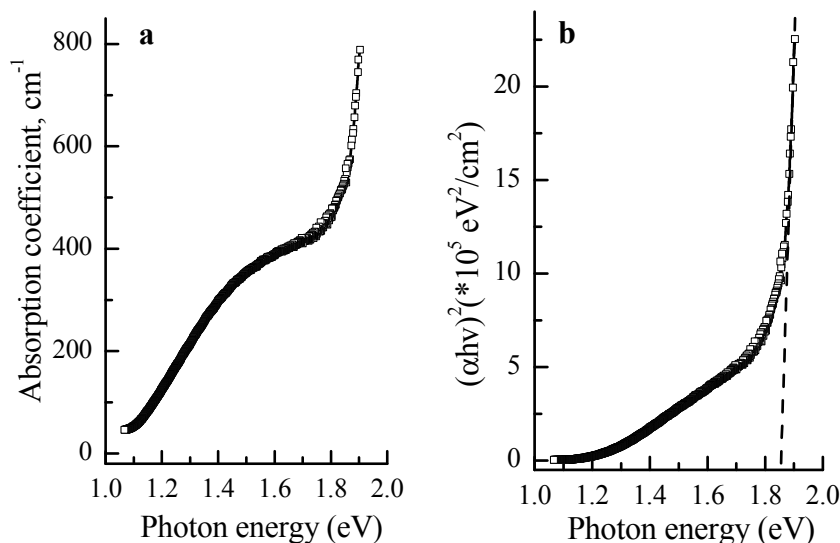


**Figure 7.** (a) Typical absorption spectral edge obtained at 300 K; (b) assumed direct renormalized absorption spectrum versus photon energy for  $\text{TlGaSn}_2\text{Se}_6$ .

The complex shape of the absorption edge is clearly seen (Figure 7b). A significant difference in the spectral distribution of the absorption coefficient for  $\text{TlGaSe}_2$  [52] and  $\text{TlGaSn}_2\text{Se}_6$  crystals is observed at energies below the beginning of inter-band transitions, in the spectral range of about  $\sim 790$  nm (1.57 eV). However, due to a great number of intrinsic defects with energy levels below the conduction band gap, a clear separation of the direct and indirect transitions is not possible. Moreover, the huge anharmonic phonon contribution that is typical for chalcogenide crystals may also be superimposed. Similar absorption spectra were obtained in [53] for  $\text{TlGaSe}_2$  with Fe admixtures. The authors suggest

that these absorption bands are associated with the substitution of the “host” metal atoms by Fe atoms. It was suggested in Ref. [54] that the substitution is possible because the ionic radii are nearly equal, 0.63 Å for Fe<sup>3+</sup> and 0.61 Å for Ga<sup>3+</sup>. Therefore, it may be assumed that the ~790 nm peak (~1.57 eV) in the TlGaSn<sub>2</sub>Se<sub>6</sub> crystals is related to the statistical substitution of Ga<sup>3+</sup> (0.61 Å) ions with Sn<sup>4+</sup> ions (0.69 Å), which agrees with the data reported in [19,28].

### 3.1.4. Nonlinear Optical Properties

We have performed studies of the third order nonlinear optical properties of the TlGaSn<sub>2</sub>Se<sub>6</sub> crystal, focusing on the third harmonic generation (THG) of a fundamental 1064 nm Nd:YAG pulse laser (pulse duration about 7 ns, frequency repetition about 10 Hz) operating in reflected geometry (see Figure 8), with energy ranging up to 200 J/m<sup>2</sup>. For investigations of the influence of photoinduced radiation on the THG intensity, we have used the continuous wave (cw) laser (532 nm). The Nd:YAG laser (1064 nm) interacting with crystals surface generated its THG signal, which was spectrally separated by a UV optical filter at 355 nm from fundamental ones before the Hamamatsu photomultiplier.

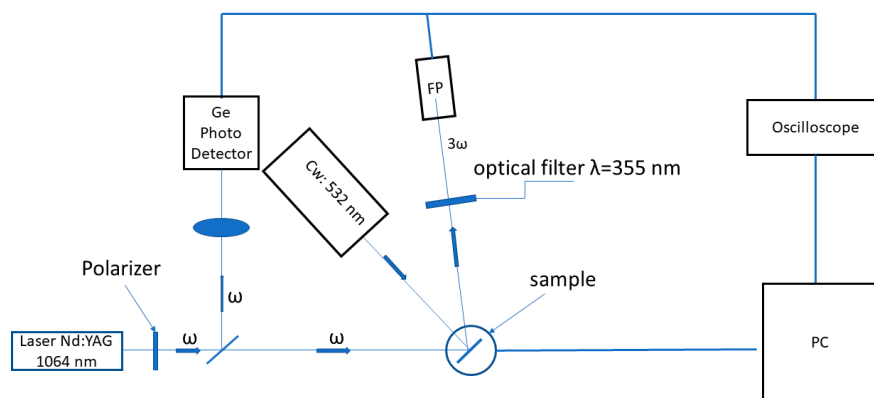


**Figure 8.** Principal set-up for measurements of the reflected photoinduced third harmonic generation (THG).

Beginning from 170 J/m<sup>2</sup> (Figure 9), a sharp increase of the THG intensity appears. As a reference compound, we have chosen a Cu<sub>2</sub>ZnSiSe<sub>4</sub> crystal that was calibrated earlier [55–57]. Figure 9 indicates that such technique allows evaluating the efficiency of the THG intensity determined from angle dependent maxima with respect to the reference sample.

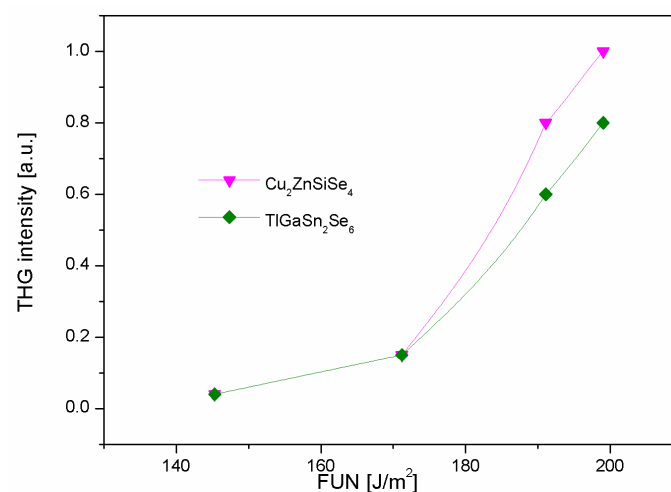


**Figure 9.** Third harmonic generation intensity for TlGaSn<sub>2</sub>Se<sub>6</sub> (Note: Cu<sub>2</sub>ZnSiSe<sub>4</sub> is used for reference).

The nonlinear THG optical effects may exist both in centrosymmetric, as well as acentric media. It is principally different to the second harmonic generation (SHG), which requires the existence of non-centrosymmetry. However, using external photopolarization, it is possible to additionally operate by the THG efficiency. We explore changes in the THG intensity under influence of the external laser operating with polarized light (green 532 cw lasers). We chose wavelengths of the photoinduced light that are higher than the energy gap value. Following the absorption coefficients measured at 355 nm for the titled crystal corresponding to the THG signal, we have evaluated that the light penetration depth is about 100 nm. The observed laser stimulated changes in the THG are determined alterations of dipole moments, and particularly by vectorial difference between the excited and ground state moments (Equation (2)). To explain such effects, we present the oversimplified expression describing the microscopic hyperpolarizabilities that are responsible for the THG effects as follows:

$$\gamma_{ijkl} \cong \frac{\vec{\mu}_i \vec{\mu}_j \Delta \vec{\mu}_k \Delta \vec{\mu}_l}{E_g^4} \quad (2)$$

where  $\Delta \mu_i$  are transition dipole moments vectorial differences between the excited and ground state dipole moments for appropriate states.

It is well known that the THG intensity is determined by third rank hyperpolarizabilities. Since we observe significant light induced alterations of the THG, it indicates the existence of effective changes in appropriate materials constants (caused by light induced photopolarization).

Additional source of the effect is caused by space redistribution of the free carriers, which give additional contribution to the changes in the THG. In Figure 10 are presented principal results devoted to the laser induced changes of the THG. The red colour corresponds to the values of the THG immediately after irradiation (up to 1 s). The blue colour corresponds to the effect after stabilisation, which rated up to 200–400 s. The stabilisation of the laser operated changes is caused by the redistribution of the photoinduced layers due to the photopolarization, photothermal effects, and free carriers. The  $\text{Cu}_2\text{ZnSiSe}_4$  crystals are used only as a reference. It is clear that, at the beginning, the changes for the reference crystals are absent and only after few minutes corresponding changes were observed. It is crucial that such behaviour is contrasted with the reference  $\text{Cu}_2\text{ZnSiSe}_4$  crystals. This fact may confirm the principal difference of the laser induced THG for different chalcogenides.

Contrary to other quaternary chalcogenides, the  $\text{TlInGe}_2\text{S}_6$  crystal photoinduced THG intensity signal decreases during photo-inducing treatment (see Figure 10). This behavior provides a unique opportunity to change the intensity of the THG by additional laser irradiation. This  $\text{TlInGe}_2\text{Se}_6$  crystal property gives the possibility to use the titled compound in the construction of advanced optoelectronic devices.

Due to the extremely high degree of the phonon anharmonic components for such a kind of materials [58], which is described by the third order polar tensors, one can expect a possibility to occur of the additional contributions to the hyperpolarizabilities.

The principal manifestation of this effect is presented in the Figure 10. Following these results, one can see that for the  $\text{Cu}_2\text{ZnSiSe}_4$  crystals the effect is absent immediately after illumination and is observed only after relaxation over 20–30 s. However, for the studied crystals, this effect is appeared immediately after the illumination. This peculiarity may be explained by different photothermal formed space gradients of free carriers and temperature, which also contribute in such a case. So, for the studied crystals, a rare opportunity occurs to modulate the intensities of the THG signal that allow us to propose the title compound to be considered a new type of nonlinear optical laser modulators [59]. It would be interesting in the future to perform the same studies for the Li-containing chalcogenide crystals revealing high laser stability and nonlinear optical (NLO) efficiencies [60].

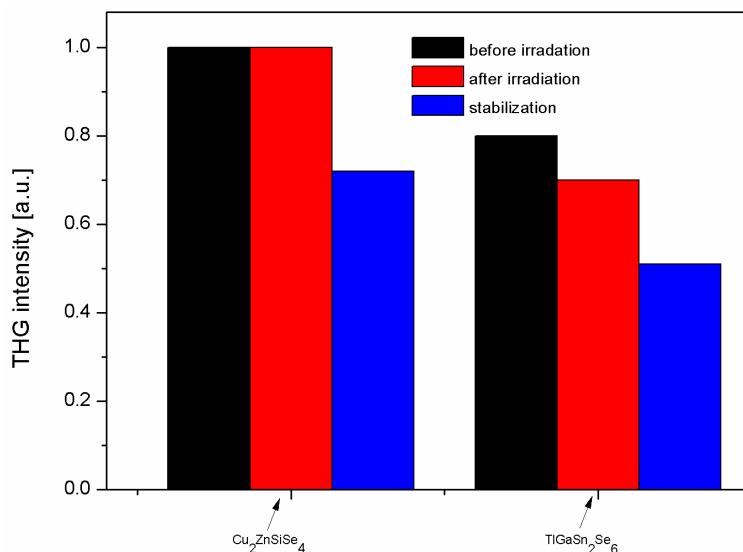


**Figure 10.** Laser stimulated changes and relaxation of the THG versus the photoinduced treatment by 532 nm cw laser for the studied crystals.

#### 4. Conclusions

Crystal structure of new quaternary selenide  $\text{TlInSn}_2\text{Se}_6$  has been determined using powder XRD method. Its crystal structure is isomorphous with a  $\text{TlInGe}_2\text{Se}_6$  structure type (non-centrosymmetric space group R3). For the  $\text{TlInSn}_2\text{Se}_6$  alloy, we have recorded the X-ray photoelectron core-level and valence-band spectra. The present XPS data indicate that all of the spectral peculiarities of the survey spectra, except for the carbon and oxygen 1s core levels and Auger KLL lines, are well assigned to the core-levels or Auger lines of atoms, which compose the  $\text{TlGaSn}_2\text{Se}_6$  alloy. The relative intensities of the XPS C 1s and O 1s core-level spectra of the pristine  $\text{TlGaSn}_2\text{Se}_6$  alloy surface are relatively small, and their origin is a result of adsorption from the air of hydrocarbons and oxygen-containing species. The influence of middle-energy  $\text{Ar}^+$  ions on the XPS spectra of the  $\text{TlInSn}_2\text{Se}_6$  alloy surface has been investigated. The present XPS data indicate that the alloy surface is rather rigid with respect to the influence on it the X-ray irradiation. An evaluation of the ionicity degree of the chemical Tl–Se bonds in the  $\text{TlGaSn}_2\text{Se}_6$  compound indicates that it is very close to that in the related quaternary selenide  $\text{TlInGe}_2\text{Se}_6$ . Furthermore, a comparison on a common energy scale of the X-ray emission Se  $K\beta_2$  band, retrieving information on the energy distribution of the Se 4p states, with the X-ray photoelectron valence-band spectrum reveals that the main contributions of the Se 4p states occurs in the upper portion of the valence band of  $\text{TlInSn}_2\text{Se}_6$ , with their substantive contributions in other portions of the band as well. Optical band gap energy for directly allowed transitions was determined from the spectral distribution of the absorption coefficient ( $E_g^d = 1.86$  eV). The position of the deep admixture level is estimated as  $\sim 1.57$  eV. New quaternary selenide  $\text{TlInSn}_2\text{Se}_6$  proved to be a very good nonlinear material that is sensitive to photoinduction operations (see Figure 10), making it to be interesting from the point of view of potential applications.

**Author Contributions:** Oleh V. Parasyuk, Oksana V. Tsisar, Lyudmyla V. Piskach—crystal preparation, Volodymyr S. Babizhetskyy, Volodymyr O. Levytskyy—XRD measurements and structure determination, Oleg Y. Khyzhun—X-ray photoelectron core-level and valence-band spectra studies, Jaroslaw Jedryka, Artur Maciag—THG measurements, Galyna L. Myronchuk—optical band determination, Iwan V. Kityk, Michal Piasecki—idea and article writing.

**Conflicts of Interest:** The authors declare no conflict of interest. The founding sponsors had no role in the design of the study; in the collection, analyses, or interpretation of data; in the writing of the manuscript, and in the decision to publish the results.

## References

1. Yursek, N.S.; Kavas, H.; Gansaly, N.M.; Ozkan, H. Trapping center parameters of TlGaSe<sub>2</sub> layered crystals. *Phys. B* **2004**, *344*, 249.
2. Fedotov, A.K.; Tarasik, M.I.; Mammadov, T.G.; Svito, I.A.; Zhukowski, P.; Koltunowicz, T.N.; Seyidov, M.Y.; Suleymanov, R.A.; Grivickas, V. Electrical properties of the layered single crystals TlGaSe<sub>2</sub> and TlInSe<sub>2</sub>. *Prz. Elektrotech.* **2012**, *88*, 301–304.
3. Delgado, G.E.; Mora, A.J.; Pérez, F.V.; González, J. Growth and crystal structure of the layered compound TlGaSe<sub>2</sub>. *Cryst. Res. Technol.* **2007**, *42*, 663–666. [[CrossRef](#)]
4. Shaban, H.T. Measurements of transport properties of TlGaSe<sub>2</sub> crystals. *Mater. Chem. Phys.* **2010**, *119*, 131–134. [[CrossRef](#)]
5. Hancias, M.P.; Anagnostopoulos, A.N.; Kambas, K.; Spyridelis, J. Electrical and optical properties of as-grown TlInSe<sub>2</sub>, TlGaSe<sub>2</sub> and TlGaS<sub>2</sub> single crystals. *Mater. Res. Bull.* **1992**, *27*, 25–38. [[CrossRef](#)]
6. Qasrawi, A.F.; Gasanly, N.M. Electrical conductivity and Hall mobility in p-type TlGaSe<sub>2</sub> crystals. *Mater. Res. Bull.* **2004**, *39*, 1353–1359. [[CrossRef](#)]
7. Liu, Z.; Peters, J.A.; Zang, C.; Cho, N.K.; Wessels, B.W.; Johnsen, S.; Peter, S.; Androulakis, J.; Kanatzidis, M.G.; Song, J.H.; et al. Tl-based wide gap semiconductor materials for x-ray and gamma ray detection. *Proc. SPIE* **2011**, *8018*, 80180H. [[CrossRef](#)]
8. Johnsen, S.; Liu, Z.; Peters, J.A.; Song, J.H.; Peter, S.C.; Malliakas, C.D.; Cho, N.K.; Jin, H.; Freeman, A.J.; Wessels, B.W.; et al. Thallium Chalcogenide-Based Wide-Band-Gap Semiconductors: TlGaSe<sub>2</sub> for Radiation Detectors. *Chem. Mater.* **2011**, *23*, 3120–3128. [[CrossRef](#)]
9. Abasova, A.Z.; Kerimova, E.M.; Muradova, G.A.; Pashaev, A.M. Ionizing irradiation of photoresistors and diode structure on the base of TlGaSe<sub>2</sub> and TlInSe<sub>2</sub> single crystals. *Phys. Conf. Ser.* **1998**, *152*, 983–988.
10. Badikov, V.V.; Tyulyupa, A.G.; Shevyrdyaeva, G.S.; Sheina, S.G. Solid-Solutions in the AgGaS<sub>2</sub>-GeS<sub>2</sub> and AgGaSe<sub>2</sub>-GeSe<sub>2</sub> Systems. *Inorg. Mater.* **1991**, *21*, 177–180.
11. Al-Harbi, E.; Wojciechowski, A.; AlZayed, N.; Parasyuk, O.V.; Gondek, E.; Armatys, P.; El-Naggar, A.M.; Kityk, I.V.; Karasinski, P. IR laser induced spectral kinetics of AgGaGe<sub>3</sub>Se<sub>8</sub>: Cu chalcogenide crystals. *Spectrochim. Acta A* **2013**, *111*, 142–149. [[CrossRef](#)] [[PubMed](#)]
12. Parasyuk, O.V.; Fedorchuk, A.O.; Gorgut, G.P.; Khyzhun, O.Y.; Wojciechowski, A.; Kityk, I.V. Crystal growth, electron structure and photo induced optical changes in novel Ag<sub>x</sub>Ga<sub>x</sub>Ge<sub>1-x</sub>Se<sub>2</sub> (x = 0.333, 0.250, 0.200, 0.167) crystals. *Opt. Mater.* **2012**, *35*, 65–73. [[CrossRef](#)]
13. Petrov, V.; Noack, F.; Badikov, V.; Shevyrdyaeva, G.; Panyutin, V.; Chizhikov, V. Phase-matching and femtosecond difference-frequency generation in the quaternary semiconductor AgGaGe<sub>5</sub>Se<sub>12</sub>. *Appl. Opt.* **2004**, *43*, 4590–4597. [[CrossRef](#)] [[PubMed](#)]
14. Schunemann, P.G.; Zawilski, K.T.; Pollak, T.M. Horizontal gradient freeze growth of AgGaGeS<sub>4</sub> and AgGaGe<sub>5</sub>Se<sub>12</sub>. *J. Cryst. Growth* **2006**, *287*, 248–251. [[CrossRef](#)]
15. Badikov, V.; Mitin, K.; Noack, F.; Panyutin, V.; Petrov, V.; Seryogin, A.; Shevyrdyaeva, G. Orthorhombic nonlinear crystals of Ag<sub>x</sub>Ga<sub>x</sub>Ge<sub>1-x</sub>Se<sub>2</sub> for the mid-infrared spectral range. *Opt. Mater.* **2009**, *31*, 590–597. [[CrossRef](#)]
16. Chirilă, A.; Buecheler, S.; Pianezzi, F.; Bloesch, P.; Gretener, C.; Uhl, A.R.; Fella, C.; Kranz, L.; Perrenoud, J.; Seyrling, S.; et al. Highly efficient Cu (In, Ga) Se<sub>2</sub> solar cells grown on flexible polymer films. *Nat. Mater.* **2011**, *10*, 857–861. [[CrossRef](#)] [[PubMed](#)]
17. Mozolyuk, M.Y. Phase Equilibria and Properties of Phases in the Tl<sub>2</sub>X-BIIX-DIVX<sub>2</sub> and TICIIIX<sub>2</sub>-DIVX<sub>2</sub> Systems (BII-Hg,Pb; CIII-Ga,In; DIV-Si,Ge,Sn; X-S,Se). Ph.D. Thesis, Uzhhorod National University, Uzhhorod, Ukraine, 2013.
18. Mozolyuk, M.Y.; Piskach, L.V.; Fedorchuk, A.O.; Kityk, I.V.; Olekseyuk, I.D.; Parasyuk, O.V. Phase diagram of the quasi-binary system TlInSe<sub>2</sub>-SnSe<sub>2</sub>. *J. Alloys Compd.* **2011**, *509*, 2693–2696. [[CrossRef](#)]
19. Franiv, A.V.; Kushnir, O.S.; Girnyk, I.S.; Franiv, V.A.; Kityk, I.; Piasecki, M.; Plucinski, K.J. Growth, crystal structure, thermal properties and optical anisotropy of Tl<sub>4</sub>CdI<sub>6</sub> single crystals. *Ukr. J. Opt.* **2013**, *14*, 6–14. [[CrossRef](#)]
20. Myronchuk, G.L.; Davydyuk, G.E.; Parasyuk, O.V.; Khyzhun, O.Y.; Andrievski, R.A.; Fedorchuk, A.O.; Danylchuk, S.P.; Piskach, L.V.; Mozolyuk, M.Y. Tl<sub>1-x</sub>In<sub>1-x</sub>Sn<sub>x</sub>Se<sub>2</sub> (x = 0, 0.1, 0.2, 0.25) single-crystalline alloys as promising non-linear optical materials. *J. Mater. Sci. Mater. Electron.* **2013**, *24*, 3555–3563. [[CrossRef](#)]

21. Myronchuk, G.L.; Zamurueva, O.V.; Parasyuk, O.V.; Piskach, L.V.; Fedorchuk, A.O.; AlZayed, N.S.; El-Naggar, A.M.; Ebothe, J.; Lis, M.; Kityk, I.V. Structural and optical properties of novel optoelectronic  $Tl_{1-x}In_{1-x}SixSe_2$  single crystals. *J. Mater. Sci. Mater. Electron.* **2014**, *25*, 3226–3232. [[CrossRef](#)]
22. Barchij, I.; Sabov, M.; El-Naggar, A.M.; AlZayed, N.S.; Albassam, A.A.; Fedorchuk, A.O.; Kityk, I.V.  $Tl_4SnS_3$ ,  $Tl_4SnSe_3$  and  $Tl_4SnTe_3$  crystals as novel IR induced optoelectronic materials. *J. Mater. Sci. Mater. Electron.* **2016**, *27*, 3901–3905. [[CrossRef](#)]
23. Kityk, I.V.; Ozga, K.; Ren, J.; Wagner, T.; Frumar, M. Optical and DC-electric poling on  $Ag_x$  ( $X = Cl, I$ )-Doped chalcogenide glasses. *Laser Phys.* **2008**, *18*, 780–782. [[CrossRef](#)]
24. Kityk, I.V. IR-stimulated second harmonic generation in  $Sb_2Te_2$  Se-BaF<sub>2</sub>-PbCl<sub>2</sub> glasses. *J. Mod. Opt.* **2004**, *51*, 1179–1189.
25. Isaenko, L.; Yelissev, A.; Lobanov, S.; Krinitsyn, P.; Petrov, V.; Zondy, J.J. Ternary chalcogenides  $LiBC_2$  ( $B = In, Ga; C = S, Se, Te$ ) for mid-IR nonlinear optics. *J. Non-Cryst. Solids* **2006**, *352*, 2439–2443. [[CrossRef](#)]
26. Isaenko, L.; Yelissev, A.; Lobanov, S.; Vedenyapin, V.; Krinitsyn, P.; Petrov, V. Properties of  $LiGa_{0.5}In_{0.5}Se_2$ : A quaternary chalcogenide crystal for nonlinear optical applications in the mid-IR. *Crystals* **2016**, *6*, 85. [[CrossRef](#)]
27. Nakamura, Y.; Aruga, A.; Nakai, I.; Nagashima, K. The Crystal structure of a new thiosilicate of thallium,  $TlInSi_4$ . *Bull. Chem. Soc. Jpn.* **1984**, *57*, 1718–1722. [[CrossRef](#)]
28. Myronchuk, G.; Danylchuk, S.; Parasyuk, O.V.; Piskach, L.V.; Fedorchuk, A.O. Spectral and conductivity features of novel ternary  $Tl_{1-x}In_{1-x}Sn_xS_2$  crystals. *Cryst. Res. Technol.* **2013**, *48*, 464–475. [[CrossRef](#)]
29. Yohannan, J.P.; Vidyasagar, K. Syntheses, structural variants and characterization of  $AlnM'S_4$  ( $A = \text{alkali metals, Tl}; M' = Ge, Sn$ ) compounds; facile ion-exchange reactions of layered  $NaInSn_4$  and  $KInSn_4$  compounds. *J. Solid State Chem.* **2016**, *238*, 291–302. [[CrossRef](#)]
30. Nakamura, Y.; Nakai, I.; Nagashima, K. Preparation and characterization of the new quaternary chalcogenides  $Tl-III-IV-S_4$  ( $III = Al, Ga, In; IV = Si, Ge$ ). *Mater. Res. Bull.* **1984**, *19*, 563–570. [[CrossRef](#)]
31. Khyzhun, O.Y.; Parasyuk, O.V.; Tsisar, O.V.; Piskach, L.V.; Myronchuk, G.L.; Levytskyy, V.O.; Babizhetskyy, V.S. New quaternary thallium indium germanium selenide  $TlInGe_2Se_6$ : Crystal and electronic structure. *J. Solid State Chem.* **2017**, *254*, 103–108. [[CrossRef](#)]
32. Khyzhun, O.Y.; Babizhetskyy, V.S.; Kityk, I.V.; Piasecki, M.; Lakshminarayana, G.; Levytskyy, V.O.; Tsisar, O.V.; Piskach, L.V.; Parasyuk, O.V.; Naggar, A.M.E.L.; et al. Albassam Thallium indium germanium sulphide ( $TlInGe_2S_6$ ) as efficient materials for nonlinear optical operation. *J. Alloys Compd.* submitted.
33. Khyzhun, O.Y.; Fedorchuk, A.O.; Kityk, I.V.; Piasecki, M.; Mozolyuk, M.Y.; Piskach, L.V.; Parasyuk, O.V.; ElNaggar, A.M.; Albassam, A.A.; Karasinski, P. Electronic structure and laser induced piezoelectricity of a new quaternary compound  $TlInGe_3S_8$ . *Mater. Chem. Phys.* **2017**. [[CrossRef](#)]
34. Akselrud, L.; Grin, Y. WinCSD: Software package for crystallographic calculations (Version 4). *J. Appl. Crystallogr.* **2014**, *47*, 803–805. [[CrossRef](#)]
35. Rajagopal, S.; Bharaneswari, M.; Nataraj, D.; Khyzhun, O.Y.; Djaoued, Y. Crystal structure and electronic properties of facile synthesized  $Cr_2O_3$  nanoparticles. *Mater. Res. Express* **2016**, *3*, 095019. [[CrossRef](#)]
36. Bozhko, V.V.; Tretyak, A.P.; Parasyuk, O.V.; Ocheretova, V.A.; Khyzhun, O.Y. X-ray spectroscopy study of the electronic structure of non-centrosymmetric  $Ag_2 CdSnS_4$  single crystal. *Opt. Mater.* **2014**, *36*, 1396–1401. [[CrossRef](#)]
37. Piasecki, M.; Myronchuk, G.L.; Zamurueva, O.V.; Khyzhun, O.Y.; Parasyuk, O.V.; Fedorchuk, A.O.; Albassam, A.; El-Naggar, A.M.; Kityk, I.V. Huge operation by energy gap of novel narrow band gap  $Tl_{1-x}In_{1-x}BxSe_2$  ( $B = Si, Ge$ ): DFT, X-ray emission and photoconductivity studies. *Mater. Res. Express* **2016**, *3*, 025902. [[CrossRef](#)]
38. Parasyuk, O.V.; Pavlyuk, V.V.; Khyzhun, O.Y.; Kozer, V.R.; Myronchuk, G.L.; Sachanyuk, V.P.; Dmytriv, G.S.; Krymus, A.; Kityk, I.V.; El-Naggar, A.M.; et al. Synthesis and structure of novel  $Ag_2 Ga_2 SiSe_6$  crystals: Promising materials for dynamic holographic image recording. *RSC Adv.* **2016**, *6*, 90958–90966. [[CrossRef](#)]
39. Bekenev, V.L.; Bozhko, V.V.; Parasyuk, O.V.; Davydyuk, G.E.; Bulatetska, L.V.; Fedorchuk, A.O.; Kityk, I.V.; Khyzhun, O.Y. Electronic structure of non-centrosymmetric  $AgCd_2GaS_4$  and  $AgCd_2GaSe_4$  single crystals. *J. Electron Spectrosc. Relat. Phenom.* **2012**, *185*, 559–566. [[CrossRef](#)]
40. Khyzhun, O.Y.; Zaulychny, Y.V.; Zhurakovskiy, E.A. Electronic structure of tungsten and molybdenum germanides synthesized at high pressures. *J. Alloys Compd.* **1996**, *244*, 107–112. [[CrossRef](#)]

41. Parasyuk, O.; Piskach, L.; Levytsky, V.; Babizhetskyy, V. TlGaSn<sub>2</sub>Se<sub>6</sub>—A new quaternary representative of the TlInGe<sub>2</sub>Se<sub>6</sub> structure type. In Proceedings of the XIII International Conference on Crystal Chemistry of Intermetallic Compounds, Lviv, Ukraine, 25–29 September 2016; p. 89.
42. Levytsky, V.; Babizhetskyy, V.; Piskach, L.; Parasyuk, O. Crystal structure of new quaternary selenide TlInGe<sub>2</sub>Se<sub>6</sub>. In Proceedings of the VIII International Workshop “Relaxed, Nonlinear and Acoustic Optical Processes and Materials, Lutsk–Lake Svityaz, Ukraine, 1–4 June 2016; pp. 51–53.
43. Brandenburg, K. *DIAMOND, Crystal Impact*; H. Putz & K. Brandenburg GbR: Bonn, Germany, 2006.
44. Dobrovolsky, V.D.; Khyzhun, O.Y.; Sinelnichenko, A.K.; Ershova, O.G.; Solonin, Y.M. XPS study of influence of exposure to air on thermal stability and kinetics of hydrogen decomposition of MgH<sub>2</sub> films obtained by direct hydrogenation from gaseous phase of metallic Mg. *J. Electron Spectrosc. Relat. Phenom.* **2017**, *215*, 28–35. [[CrossRef](#)]
45. Moulder, J.F.; Stickle, W.E.; Sobol, P.E.; Bomben, K.E. *Handbook of X-ray Photoelectron Spectroscopy*; Chastian, J., Ed.; Perkin-Elmer: Eden Prairie, MN, USA, 1992.
46. Khyzhun, O.Y. XPS Study of the Electronic Structure of Nb<sub>1.27</sub>Se<sub>2</sub>. *Metallofiz. Noveishie Tekhnol.* **2002**, *24*, 141–149.
47. Morgan, W.E.; van Wazer, J.R. Binding energy shifts in the X-ray photoelectron spectra of a series of related Group IVa compounds. *J. Phys. Chem.* **1973**, *77*, 964–969. [[CrossRef](#)]
48. Taylor, J.A.; Lancaster, G.M.; Rabalais, J.W. Chemical reactions of N<sup>2+</sup> ions beams with group IV elements and their oxides. *J. Electron Spectrosc. Relat. Phenom.* **1978**, *13*, 435–444. [[CrossRef](#)]
49. Briggs, D.; Seach, P.M. Auger and X-ray Photoelectron Spectroscopy. In *Practical Surface Analysis*, 2nd ed.; John Wiley & Sons Ltd.: Chichester, UK, 1990; Volume 1.
50. Pankove, J.I. *Optical Process in Semiconductors*; Dover: New York, NY, USA, 1975; Volume 35.
51. Kungumadevi, L.; Sathyamoorthy, R. Structural, Electrical, and Optical Properties of PbTe Thin Films Prepared by Simple Flash Evaporation Method. *Adv. Condens. Matter Phys.* **2012**. [[CrossRef](#)]
52. Gürbulak, B.; Duman, S. Urbach tail and optical characterization of gadolinium-doped TlGaSe<sub>2</sub> single crystals. *Phys. Scr.* **2008**, *77*, 025702. [[CrossRef](#)]
53. Grivickas, V.; Gavryushin, V.; Grivickas, P.; Galeckas, A.; Bikbajevs, V.; Gulbinas, K. Optical absorption related to Fe impurities in TlGaSe<sub>2</sub>. *Phys. Status Solidi A* **2011**, *208*, 2186–2192. [[CrossRef](#)]
54. Acikgoz, M.; Kazan, S.; Mikailov, F.A.; Mammadov, T.G.; Aktas, B. Structural phase transitions in Fe<sup>3+</sup> doped ferroelectric TlGaSe<sub>2</sub> crystal. *Solid State Commun.* **2008**, *145*, 539. [[CrossRef](#)]
55. Guca, A.; Levchenko, S.; Dermenji, L.; Gurieva, G.; Schorrb, S.; Syrbu, N.N.; Arushanov, E. Excitonic and band-band transitions of Cu<sub>2</sub>ZnSi<sub>4</sub> determined from reflectivity spectra. *Solid State Commun.* **2014**, *190*, 44–48. [[CrossRef](#)]
56. Rosmus, K.A.; Brant, J.A.; Wisneski, S.D.; Clark, D.J.; Kim, Y.S.; Jang, J.I.; Brunetta, C.D.; Zhang, J.H.; Srnc, M.N.; Aitken, J.A. Optical nonlinearity in Cu<sub>2</sub>CdSn<sub>4</sub> and α/β-Cu<sub>2</sub>ZnSi<sub>4</sub>: Diamond-like semiconductors with high laser-damage thresholds. *Inorg. Chem.* **2014**, *53*, 7809–7811. [[CrossRef](#)] [[PubMed](#)]
57. Valakh, M.Y.; Yuhymchuk, V.O.; Babichuk, I.S.; Havryliuk, Y.O.; Parasyuk, O.V.; Piskach, L.V.; Litvinchuk, A.P. Vibrational spectroscopy of orthorhombic Cu<sub>2</sub>ZnSi<sub>4</sub> single crystal: Low-temperature polarized Raman scattering and first principle calculations. *Vib. Spectrosc.* **2017**, *89*, 81–84. [[CrossRef](#)]
58. Kityk, I.V.; Myronchuk, G.L.; Parasyuk, O.V.; Krymus, A.S.; Rakus, P.; El-Naggar, A.M.; Albassam, A.A.; Lakshminarayana, G.; Fedorchuk, A.O. Specific features of photoconductivity and photoinduced piezoelectricity in AgGaGe<sub>3</sub>Se<sub>8</sub> doped crystals. *Opt. Mater.* **2017**, *63*, 197–206. [[CrossRef](#)]
59. Matsubara, M.; Schmehl, A.; Mannhart, J.; Schlom, D.G.; Fiebig, M. Giant third-order magneto-optical rotation in ferromagnetic EuO. *Phys. Rev. B* **2012**, *86*, 195127. [[CrossRef](#)]
60. Yelisseyev, A.; Liang, F.; Isaenko, L.; Lobanov, S.; Goloshumova, A.; Lin, Z.S. Optical properties of LiGaSe<sub>2</sub> noncentrosymmetric crystal. *Opt. Mater.* **2017**, *72*, 795–804. [[CrossRef](#)]

